ELSEVIER

Journal of Alloys and Compounds 451 (2008) 240–247

Journal of ALLOYS AND COMPOUNDS

www.elsevier.com/locate/jallcom

EPR and optical studies of $LiNbO_3$:Yb and $LiNbO_3$:Yb, Pr single crystals

T. Bodziony [a], S.M. Kaczmarek [a,*], J. Hanuza [b]

[a] *Institute of Physics, Szczecin University of Technology, Al. Piastów 17, 70-310 Szczecin, Poland*
[b] *Institute of Low Temperature and Structure Research, PAS, 2 Okólna, 50-950 Wrocław, Poland*

Available online 19 April 2007

Abstract

Some results of the absorption investigations of $LiNbO_3$:Yb^{3+}, Pr^{3+} (0.8, 0.1 wt.%) and $LiNbO_3$:Yb^{3+} (1 wt.%) single crystals were made for UV–vis and IR giving evidence on the Yb^{3+} location at Li^+ sites and Pr^{3+} location at Nb^{5+} sites. Low temperature absorption measurements have shown the presence of low energy phonons responsible for the intensity shape of the main Yb^{3+} IR absorption line as a function of the temperature. Raman spectra confirmed the observation.

We have observed several paramagnetic centers originating from both isolated Yb^{3+} and Yb^{3+} ion pairs. The observed spectral features indicate the Yb centers in both crystals exhibit triclinic C_1 symmetry. The temperature dependence of the EPR line intensity and inverse line intensity confirm the presence of coupled Yb^{3+} ion pairs besides isolated Yb^{3+} ions in both crystals. The EPR line intensity fulfils Curie–Weiss law and yields the antiferromagnetic interaction constant $\Theta = -0.6 \pm 0.3$ K and ferromagnetic interaction constant $\Theta = 2.4 \pm 0.1$ K for $LiNbO_3$:Yb^{3+} and $LiNbO_3$:Yb^{3+}, Pr^{3+} samples, respectively. The presence of co-dopant significantly changes properties of $LiNbO_3$:Yb^{3+} single crystal. The Pr co-dopant forces the substitution of Yb^{3+} ions at other possible sites in the host crystal and changes interaction between Yb ion pairs from the antiferromagnetic to ferromagnetic one.

Keywords: Ytterbium; Praseodymium; EPR; Optical spectroscopy; Raman spectra

1. Introduction

Lithium niobate $LiNbO_3$ (LN) is one of the best-studied ferroelectric, electro-optic materials [1,2]. Its structural properties and phase transitions as well as photoluminescence, Raman and ESR spectra have been studied and published in many papers, e.g. in ref. [3]. Great interest in $LiNbO_3$ is driven by its unusual non-linear electric, magnetic, and acousto-optical properties, which have been utilized for various technological applications, for example information storage, holography, lasers or amplifiers. Doping with trivalent transition ions, also rare-earth (RE) elements, has pronounced effect on some properties of LN, e.g., structure, electro-optical coefficients, light absorption. LN doped with Yb^{3+} could be realized as the efficient laser crystal [4,5]. One of the important ways to improve the laser efficiency, and other optical properties of LN doped with Yb^{3+} is co-doping. The presence of additional impurities changes the ligand field of Yb^{3+} in LN lattice, so it's electronic states, and, could influence on lattice sites substitution by Yb^{3+} ions in the host lattice.

The space group of LN crystal is $R3c$ ($C_{3v}{}^6$). It's unit cell is rhombohedral, the lattice constants at room temperature are the following: $a = 5.1483$ nm and $c = 13.8631$ Å [6,7]. The LN structure is build of the oxygen atoms arranged in planar sheets which form chains of trigonally distorted octahedra, adjoined by walls, spreading along the crystallographic c optical axis. The sequence of octahedra is: [Nb, vacancy, Li], so 1/3 amount of the octahedral is empty [3,6,7]. Characteristic feature of the LN crystal structure is that four cation sites: three octahedral sites (Li^+, Nb^{5+}, vacant octahedron) and an interstitial tetrahedral site are available for trivalent impurities in the LN host crystal. It has been shown that trivalent RE ions occupy mostly Li^+ sites and are located off-center from the regular Li^+ positions towards the structural vacancy octahedral sites along the c-axis, see e.g. [8,9]. But in several recent experimental and theoretical studies it has been shown that RE ions in LN occupy also the Nb^{5+} sites [10,12]. Generally, the RE^{3+} ions can be distributed in the crystallographically non-equivalent centers, giving rise to different sets of optical transitions [9].

* Corresponding author.
E-mail address: skaczmarek@ps.pl (S.M. Kaczmarek).

0925-8388/$ – see front matter © 2007 Elsevier B.V. All rights reserved.
doi:10.1016/j.jallcom.2007.04.189

LN is usually grown from the congruent melt compositions with Li^+ to Nb^{5+} concentration ratio of the order of 0.945 giving rise to the Li-deficient crystals that need intrinsic defects because of overall charge compensation. It is generally accepted that the Li-deficiency in $LiNbO_3$ single crystals is compensated by a certain amount of Nb^{5+} ions located at the Li^+ sites, the so-called anti-sites [10,11]. The same RE^{3+} centers appear for all possible stoichiometries (Li/Nb concentration ratio), whereas the relative concentration of such centers depends on the stoichiometry. This result indicates that the nature of the RE^{3+} centers in LN is directly related to the defects associated with the non-stoichiometric conditions.

Raman spectroscopy can be sensitive to a small change in a structure due to the non-stoichometry related to the intrinsic defects [13] or extrinsic impurities [14]. This can lead to frequency shift or broadening of Raman lines or appearance of new lines [13,15]. Mouras et al. [15] have applied Raman spectroscopy as a site-spectroscopy technique. They have used the assignment of the lowest phonon frequencies $A1(TO_1)$, $A1(TO_2)$ and $E(TO_1)$ located at 254, 276 and 153 cm^{-1} to discuss the site location of Nd^{3+}, Dy^{3+} and Er^{3+} ions. The $A_1(TO_1)$ phonon corresponds to anti-phase motion of ions in B sites generally occupied by Nb^{5+} ions against the oxygen octahedron along the ferroelectric *Z*-axis, the $A_1(TO_2)$ phonon is associated with a large displacement along *Z*-axis of ions in A sites (Li^+) in antiphase to ions in B sites, whereas the oxygen ions stay motionless [15]. The $E(TO_1)$ corresponds to the deformation of the $BO_6(NbO_6)$ framework in the (*x*, *y*) plane. Mouras et al. [15] have found RE doping pushes down the frequency for each phonon, whereas Mg doping causes opposite trends on $A_1(TO_1)$ or $E(TO_1)$ and $A_1(TO_2)$.

Palatnikov et al. [16] have investigated $LiNbO_3$ crystals doped with Tm, Er, Dy, Tb, Gd and Pr ions in a wide range of concentrations. They have found nominally pure and slightly doped LN crystals demonstrate a single-mode behavior within the region of homogeneity (~880 cm^{-1}), while in heavily doped LN crystals there is an evidence of two-mode behavior.

Chen et al. [17] have shown that Cr^{3+} can enter the Nb^{5+} sites, thus increasing the Nb_{Li} antisites concentration, while the concentration of Nb_{Li} decreases with Co^{2+} and Fe^{3+} which mainly occupy Li^+ sites. Dumping of the 152 cm^{-1} mode observed in the Raman spectrum of the Cr-doped LN he attributed to the influence of the increasing of Nb_{Li} concentration on the E(TO) phonon properties.

The electron paramagnetic resonance (EPR) spectroscopy of trivalent ytterbium in LN was investigated by Burns et al. [10], Bonardi et al. [11], Jones et al. [5], Montoya et al. [4], and Tsuboi et al. [12]. These studies indicate that the site symmetry of Yb^{3+} centers is axial (C_3) and RE ions occupy mainly the Li^+ sites. In $LiNbO_3$:Mg, Yb, Dong et al. have shown that the Yb^{3+} ions may occupy also Nb^{5+} sites because of the role of MgO co-doping [18]. Choh et al. [19] arrived at similar conclusion for Er^{3+} in Er and Mg codoped LN single crystals. Malovichko and Grachev [20,21] have shown that RE ions enter octahedral sites in LN, which may exhibit the C_3 or C_1 site symmetries.

Montoya et al. [22] have studied the cooperative luminescence in LN:Yb^{3+} (at low concentration) provided an evidence of the Yb^{3+} pairs presence in the matrix and proposed three models for Yb^{3+} ions distribution in LN, relating each model to the observed features of cooperative luminescence. The experimental results favor the Yb^{3+} distribution model in which a fraction of dopant ions (about 10.4% of the Yb^{3+} ions) form pairs with one Yb^{3+} ion placed at the Li^+ site and another one at the Nb^{5+} site, while the rest of the Yb^{3+} ions are randomly distributed at the Li^+ sites.

Our previous studies focused on investigation of LN single crystals doped with Yb^{3+} ions [23] and doped with Yb^{3+} and co-doped with Pr^{3+} [24]. We have found that Yb^{3+} ions occupy mainly sites with lower C_1 symmetry in both LN:Yb, Pr and LN:Yb crystals. In this paper we concentrate ourselves on comparison of the EPR, and optical spectroscopy results of LN:Yb (1 wt.%) and LN:Yb, Pr (0.8, 0.1 wt.%) crystals. In case of optical spectroscopy we compare the absorption spectra of the crystals to the spectra of LN:Pr (1 wt.%) and LN:Yb, Pr (0.8, 0.5 wt.%) single crystals. Some conclusions were made also from Raman spectra of LN:Nd, Mg (2, 6 wt.%), LN:Nd, Yb (0.5, 0.7 wt.%) and LN:Er (0.3 wt.%) single crystals.

2. Experimental

Pure LN and LN:Pr (1 wt.%), LN:Nd, Mg (2, 6 wt.%), LN:Nd, Yb (0.5, 0.7 wt.%), LN:Er (0.3 wt.%), LN:Yb (1 wt.%) and LN:Yb, Pr (0.8, 0.1 wt.%) and LN:Yb, Pr (0.8, 0.5 wt.%) single crystals were grown along the *c*-axis from the congruent melt by the Czochralski method in the Institute of Electronic Materials Technology, Warsaw, Poland. After mixing of adequate amounts of reagents the mixture was calcined at 1373 K for 6 h. The Nd_2O_3, MgO, Er_2O_3, Yb_2O_3 and Pr_2O_3 were added to the charge of congruent melt with the Li/Nb ratio equal 0.94, prior to synthesis at elevated temperatures. The growth conditions were the following: growth rate: 1–2 mm/h, rotation rate: 5–20 rpm, axial temperature gradient over melt: 10–30 ° cm^{-1}, atmosphere: air. A more detailed description of the applied growth process is presented elsewhere [25]. The as grown crystals were regular and free of macroscopic defects [26]. The samples for optical investigations were cut out from the crystals perpendicularly to *c*-axis, and then both sides polished to the thickness of about 1 mm. The samples for EPR experiments had the form of rectangular prisms of dimensions 3.1 mm × 2.7 mm × 1.5 mm and 3.0 mm × 1.6 mm × 3.2 mm, for LN:Yb and LN:Yb, Pr, respectively, with surfaces perpendicular to the crystalographical axes determined from XRD measurements.

Unpolarized absorption spectra were recorded in the spectral range 190–3100 nm at temperatures 16–300 K using Cary-5E spectrophotometer in Kyoto Sangyo University, Japan for low temperature optical density measurements and Lambda-900 of Perkin-Elmer in the Institute of Optoelectronics, MUT for room transmission spectra. Photoluminescence measurements were carried out using SS-900 Edinburgh Inc. spectrophotometer in the Institute of Optoelectronics, MUT.

X(YZ)Y Raman spectra were recorded for LN:Nd, Mg (2, 6 wt.%), LN:Nd, Yb (0.5, 0.7 wt.%) and LN:Er (0.3 wt.%) single crystals, two first of them being irradiated with γ-quanta with a dose of 10^7 Gy, for A and E modes within a resolution 0.56 cm^{-1}. SPEX 1403 Raman spectrometer was used applying right-angle scattering geometry and the 488 nm line of an Ar^+ laser.

EPR spectra were recorded using Bruker E 500 X-band spectrometer ($\nu \sim 9.4$ GHz) with 100 kHz field modulation equipped with Oxford flow cryostat for measurements at temperatures from liquid nitrogen temperature down to 4 K and a goniometer to measure the angular dependence of the EPR spectra.

3. Results and discussion

3.1. Optical spectroscopy measurements

Fig. 1 presents the absorption coefficient of LN single crystals pure and doped with Yb (1 wt.%), Pr (1 wt.%), Yb and Pr (0.8, 0.1 wt.%), and, Yb and Pr (0.8, 0.5 wt.%) measured at room temperature. Reach spectrum one can observe with the absorption bands characteristic of Yb^{3+} (850–1100 nm band, $^2F_{7/2}$–$^2F_{5/2}$ transition) and Pr^{3+} ions. The intensity of the Pr^{3+} related absorption bands strongly depend on the Pr^{3+} concentration, and the shifting of the fundamental absorption edge (FAE) is observed with the increase of the Pr^{3+} concentration. As one can see LN crystals co-doped with Pr^{3+} reveal higher intensity of OH^- absorption line, centred at about 2871 nm, due to the necessity of charge compensation of trivalent RE ions introduced for Li^+ and/or Nb^{5+} (see inset in Fig. 1). The band is twice higher than usually detected for RE doped LN crystals [12]. We have observed much higher OH^- absorption band intensity in Pr^{3+}-doped and co-doped crystals as compare to pure and singly doped with Yb^{3+}, and the increase of the intensity with increasing Pr^{3+} concentration. This suggests the Yb^{3+} ion with ionic radius 0.868 nm is substituted for Li^+ ion with smaller ionic radius of 0.76 nm, while Pr^{3+} ion, with larger ionic radius of 0.99 nm, is substituted for Nb^{5+} ion with much smaller ionic radius 0.64 nm. The latter substitution leads to the octahedra being deformed and creation of negatively charged defects of $(Pr^{3+}{}_{Nb^{5+}})^{2-}$ type that require charge compensation by positively charged $(OH^-{}_{O^{2-}})^{+}$ ones in $Yb^{3+}+Pr^{3+}$ co-doped LN crystal.

The low temperature absorption spectra consist of intense and sharp bands due to the $^2F_{7/2}$–$^2F_{5/2}$ electronic transition of Yb^{3+} and weak bands due to vibronic transitions. The intense bands arise at 918.5, 955 and 980.3 nm due to $^2F_{7/2}$–$^2F_{5/2}$ of Yb^{3+}, while very weak bands are observed at 987.8, 1019, 1030 and 1057 nm, which are due to $^4H_4$–$^4G_4$ of Pr^{3+}.

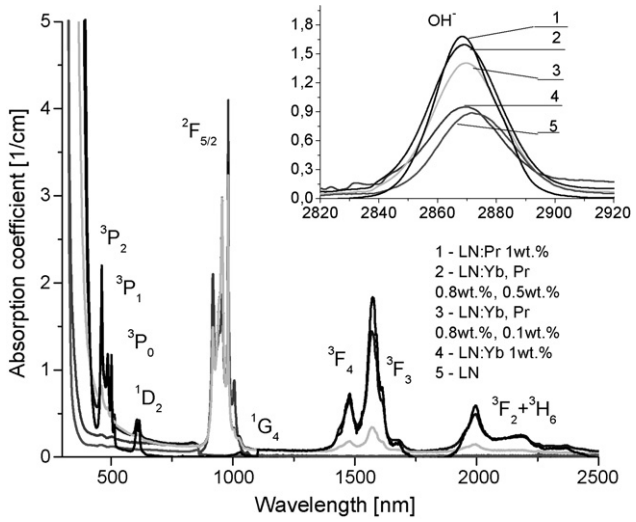

Fig. 1. Room temperature absorption coefficient of: 1, LN:Pr 1 wt.%; 2, LN:Yb Pr 0.8, 0.5 wt.%; 3, LN:Yb, Pr 0.8, 0.1 wt.%; 4, LN:Yb 1 wt.% and 5, LN pure single crystals.

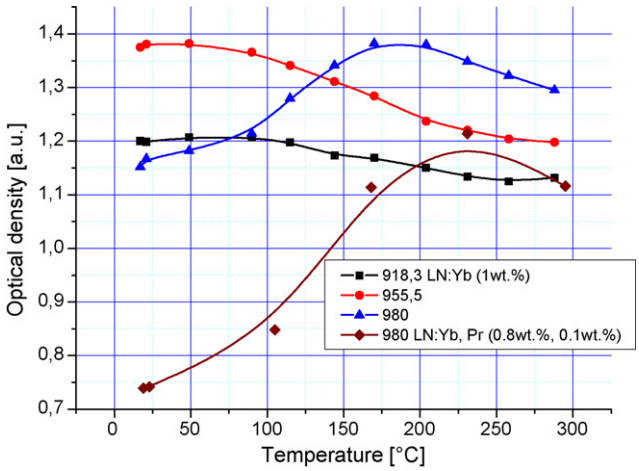

Fig. 2. Temperature dependence of 918.3, 955.5 and 980 nm absorption peaks for LN:Yb (1 wt.%) and LN:Yb, Pr (0.8, 0.1 wt.%) single crystals.

The peak position of the sharp line centred at 980 nm is different among LN crystals doped with rare-earths [12], moreover the intensity of the line strongly depend on the temperature. This is clearly observed in Fig. 2 where the intensity versus temperature is shown for the three elevated lines. The "normal" behavior of the intensity versus temperature is observed for 918.3, 918.5 and 955.5 nm lines, while "un-normal" one for 980 nm line. This "un-normal" behavior is characterized by occurring of the intensity maximum of 980 nm line at about 190 and 230 K for LN:Yb and LN:Yb, Pr, respectively. Such a maximum indicate mixed (vibronic–electronic) nature of the transition. The temperature 200 K, where a maximum of the line arise, corresponds to energy of about 140 cm^{-1}. It may be due to the existing of localized phonons in the LN crystal with this energy. This supposition was confirmed by Raman spectra investigations, were the phonons with energy within 80–300 cm^{-1} range we have clearly observed.

The shape of the curve attributed to 980 nm one can explain taking into account the possibility of the arising of RE ion pairs in the crystal. In the co-doped crystals or crystals with large dopant concentration, two kinds of Yb^{3+} ions may be present, one is Yb^{3+} accompanied by nearby rare-earth ion – perturbed Yb^{3+}, the other is Yb^{3+} located far from the rare-earth ion – isolated. The energy levels of the perturbed Yb^{3+} ions are shifted from those of the isolated Yb^{3+} ions giving rise to the small shifting (~0.1 nm) of the absorption spectra that we have previously observed [12]. Moreover, perturbed Yb^{3+} ions may be responsible for the localized phonons observed in Raman spectra. In fact, Raman spectrum of Sc^{3+}/Yb^{3+} co-doped crystal has revealed the presence of localized vibrations at 237.1 cm^{-1} [27].

3.2. Raman spectroscopy measurements

Spectra shown in Fig. 3 reveal the four $A_1(TO)$ and $E(TO_1)$, $E(TO_8)$ phonon modes obtained for different samples. The spectra resemble both the strong photoluminescence of the crystals and influence of γ-irradiation (broadening of the lines). Full Raman spectrum in the range 20–1200 cm^{-1} reveals 152 cm^{-1} $E(TO_1)$ mode, 254 cm^{-1} $A_1(TO_1)$, 274 cm^{-1}

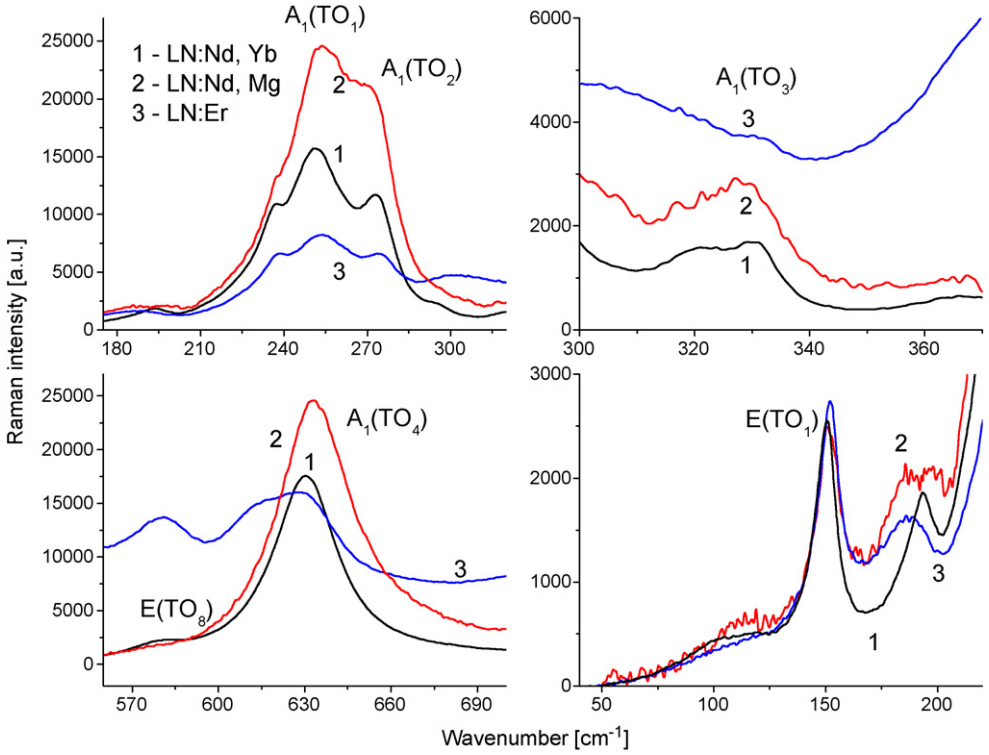

Fig. 3. Raman spectra recorded for LN:Nd, Yb (1), LN:Nd, Mg (2) and LN:Er (3) single crystals.

$A_1(TO_2)$, 331 cm^{-1} $A_1(TO_3)$, 583.1 cm^{-1} $E(TO_8)$, 630.2 cm^{-1} $A_1(TO_4)$, and 364, 432.5, 882.5 cm^{-1} A_2 modes as reported previously in [15] for LN crystal single doped with Mg, Nd, Dy and Er ions, Chen et al. [17] for LN single doped with Co, Cr and Fe and calculated by Postnikov et al. [28]. It is seen the $E(TO_1)$, $A_1(TO_1)$ and $A_1(TO_2)$ modes are significantly affected by doping. Moreover, 100, 193 and 238 cm^{-1} modes we have recognized in the Raman spectrum, being effects of γ-induced defects and extrinsic doping and co-doping. The 100 cm^{-1} mode may be attributed to γ-induced defects, although it is not excluded RE co-doping (pairs) origin. It is absent in the Raman spectrum of LN:Er crystal being not irradiated. The 180 cm^{-1} mode was observed previously by Chen et al. [17] and related to LN crystals doped with transition metal ions. The 237.1 cm^{-1} mode was observed only in double doped LN crystals as, e.g. by Mouras et al. [15] for Sc and Yb co-doped LN crystal but was not related to any physical meaning. So, basing on the above papers and comparisons of our spectra with previous one we can assign the 100 cm^{-1} Raman peak to radiation induced or co-doping (pairs) mode, the 193 cm^{-1} Raman peak to RE doping of LN crystal and 238 cm^{-1} peak as being an effect of co-doping, all the modes being localized type phonons. The presence of the modes may be connected with RE ions pairs in the LN crystals as was mentioned in Section 3.1. Er doped LN crystal shows clustered type structure revealing double $A_1(TO)$ modes [16]. Dumping of the 152 cm^{-1} mode in the Raman spectrum of the Er, Nd, Mg and Yb-co-doped LN crystal can be attributed to the influence of the increasing Nb_{Li} concentration on the E(TO) phonon properties.

3.3. EPR spectroscopy measurements

Comparative EPR absorption spectra of $LiNbO_3:Yb^{3+}$ and $LiNbO_3:Yb^{3+}$, Pr^{3+} single crystals for $T = 7.5$ and 7.4 K, respectively, are presented in Fig. 4, while EPR absorption spectra of $LiNbO_3:Yb^{3+}$, Pr^{3+} single crystal for several temperatures ranging between 5 and 42 K are shown in Fig. 5.

Representative EPR spectra of the $LN:Yb^{3+}$ sample taken at wide range angles (between 0° and 180°) in the plane perpendicular to the crystal *c*-axis (marked as *XY*) and the plane

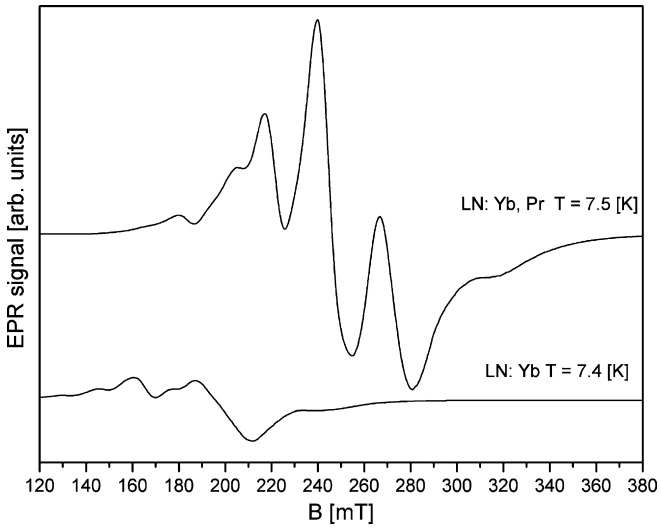

Fig. 4. Comparative EPR absorption spectra of $LiNbO_3:Yb^{3+}$ (1 wt.%) and $LiNbO_3:Yb^{3+}$, Pr^{3+} single crystals for $T = 7.4$ and 7.5 K, respectively.

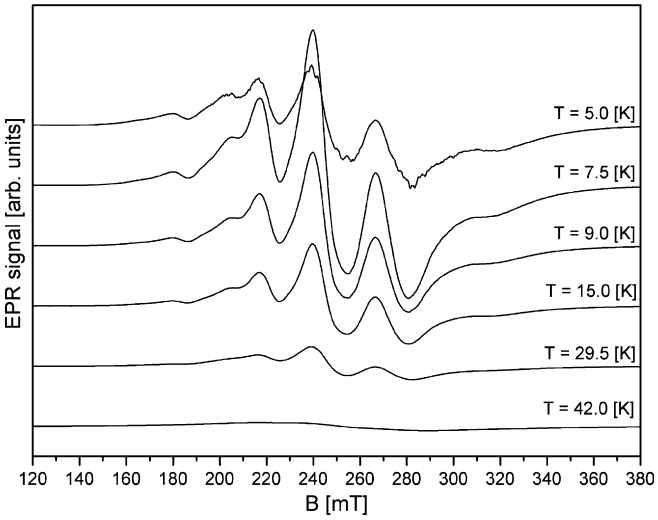

Fig. 5. EPR absorption spectra of $LiNbO_3$:Yb^{3+}, Pr^{3+} single crystal for several temperatures.

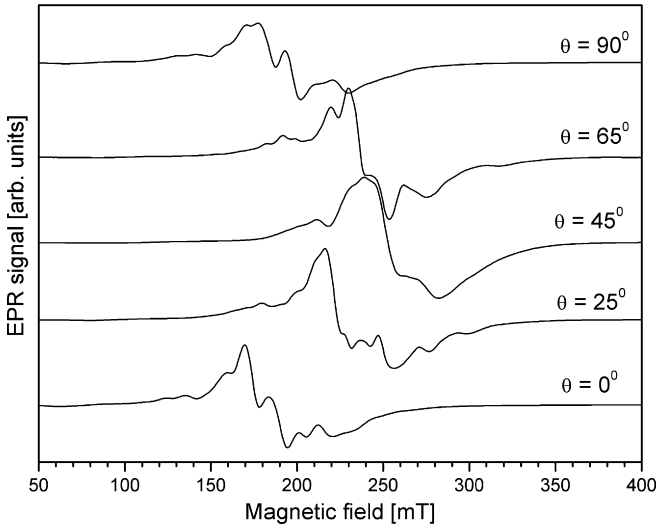

Fig. 7. Angular dependence of the EPR lines for $LiNbO_3$:Yb^{3+} crystal measured in the plane containing the crystal *c*-axis (*ZX*, $\theta = 90$ denotes the *X*-axis, $T = 6.7$ K).

containing the crystal *c*(*Z*)-axis (marked as *ZX*) are presented in Figs. 6 and 7, respectively. The most important feature of the EPR spectra of LN:Yb^{3+} seen in Figs. 4–7 is their complexity. One can observe a change in the position of EPR lines as a function of the angle in a plane containing crystal *c*-axis and other one, containing the axis perpendicular to the *c*-axis, both for LN:Yb^{3+} and LN:Yb^{3+}, Pr^{3+} samples (see Figs. 6–9). Malovichko et al. claimed that only two possible types of site symmetry of paramagnetic centers can be recognized in the $LiNbO_3$ single crystal: C_3 (axial) or C_1 site symmetries [20,21]. We have not found axial symmetry (C_3) sites because the registered EPR lines have moved in all three planes. So conclusion has been made taking into account analysis of the EPR spectra, we have observed a case of paramagnetic centers with lowest, triclinic symmetry (C_1).

The angular dependence of the EPR lines indicates that the observed spectra are a superposition of lines of various natures. The EPR spectra taken at a third plane (*ZY*) yield similar angular dependencies as shown at *ZX* plane (see Fig. 7). In case of the low symmetry sites the EPR spectra should reflect symmetry of the crystal [29]. This is clearly observed in the above-mentioned figures. Figs. 8 and 9 show representative EPR spectra of the LN doped with Yb^{3+} and Pr^{3+} crystal taken at various angels in a plane that contains the crystal *c*-axis (*XY*) and a plane perpendicular to the crystal *c*-axis (*ZY*), respectively. The spectra taken at third (*ZX*) plane are similar to those at *ZY* plane (see Fig. 9). We can observe a few strong and broad lines and additionally several weak lines, which partially could not be visible in these figures due to low resolution of the pictures, but one can clearly observe the moving of all the lines (Figs. 6–9).

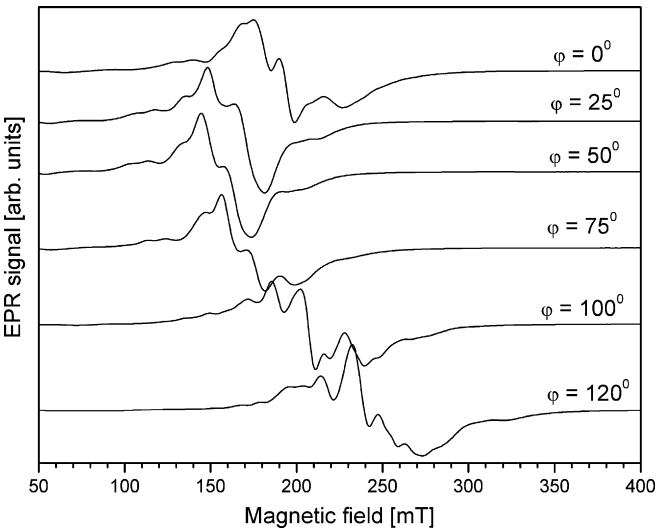

Fig. 6. Angular dependence of the EPR lines for $LiNbO_3$:Yb^{3+} crystal measured in the plane perpendicular to the crystal *c*-axis (*XY*, $\varphi = 0$ denotes the *X*-axis, $T = 6.7$ K).

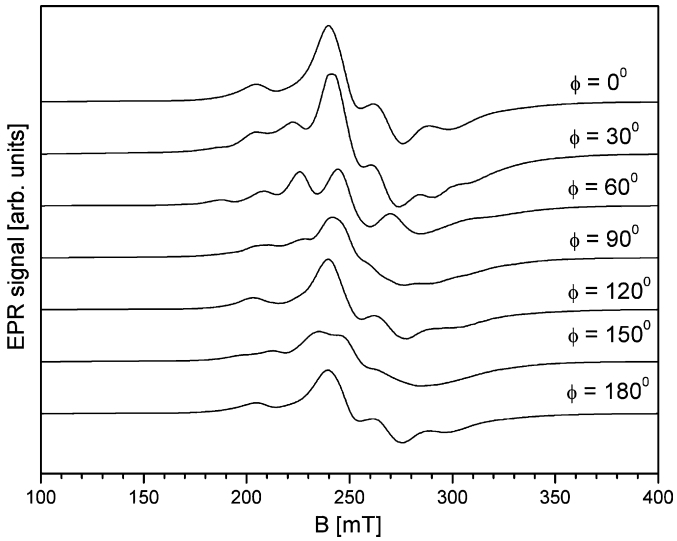

Fig. 8. Angular dependence of the EPR lines for the $LiNbO_3$:Yb^{3+}, Pr^{3+} crystal measured in the plane perpendicular to the crystal *c*-axis (*XY*, $\varphi = 0$ denotes the *X*-axis, $T = 8$ K).

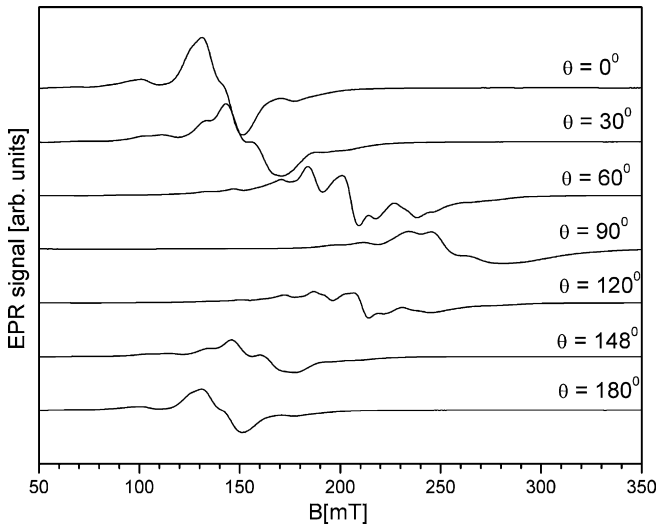

Fig. 9. Angular dependence of the EPR lines for $LiNbO_3$:Yb^{3+}, Pr^{3+} crystal measured in the plane containing the crystal *c*-axis (*ZY*, $\theta = 0$ denotes the *Z*-axis, $T = 8$ K).

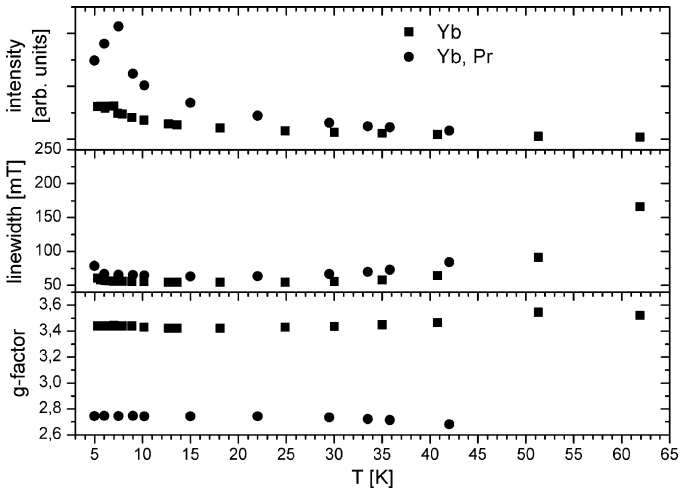

Fig. 10. Temperature dependence of the intensity (upper figure), linewidth (middle figure) and *g*-factor (lower figure) of the integral EPR line for LN:Yb^{3+} (solid squares) and LN:Yb^{3+}, Pr^{3+} crystal (solid dots).

Behaviour of the lines observed in Fig. 8 (LN:Yb^{3+}, Pr^{3+}, *XY* plane) is more complex. The strong and broad central line splits into several lines. Some of them move in the range between 180 and 350 mT. It should be noticed, moreover, that the position of the central line, visible in Fig. 8, is not stable. The line is moving slowly. It may be caused by the fact the line is a superposition of several lines, some of which are moving during rotation of a sample. The EPR spectra suggest, that we observed signals which may arise from either magnetically inequivalent paramagnetic centers of the same type or crystallographically distinct centers of the same or different type [30].

The signals originating from the isolated Yb^{3+} ions cannot be easily distinguished in LN host. The EPR spectra of Yb^{3+}-doped host crystal at helium temperature should show a single central line corresponding to the fine-structure transition (effective spin $S = 1/2$) for the even Yb^{3+} isotope with no nuclear magnetic moments ($I = 0$, natural abundance 69.6%) and/or two hyperfine transitions distributed about the central transition corresponding to nuclear spin $I = 1/2$ for odd ^{171}Yb isotope (natural abundance 14.3%) and/or six hyperfine transitions distributed about the central transition corresponding to nuclear spin $I = 5/2$ for ^{173}Yb isotope (natural abundance 16.1%) [30]. But we cannot exclude *a priori* some other possibility, like Yb ion pairs. Indeed, in some of the EPR spectra we can recognize a characteristic pattern for ion pairs. The Yb ion pairs were reported in [24,25,29]. Partially we were able successfully diagnose EPR spectra basing on the EPR signal arising from isolated Yb ions and the results of our investigations we have presented in [25,26].

In order to analyze of such complex spectra, we have investigated the temperature dependence of the integral EPR line for both crystals, i.e. temperature dependence of the intensity, linewidth, and *g*-factor. The integral EPR line is calculated using double numerical integration of the EPR signal [30]. In Fig. 10 we presented the temperature dependence of the EPR intensity line (upper figure), the peak-to-peak linewidth (middle figure) and the *g*-factor (lower figure) for both LN:Yb^{3+} (solid squares) and LN:Yb^{3+}, Pr^{3+} (solid dots) crystals, where temperature ranges from 4 to 63 and 42 K for the former and the latter crystal, respectively (see Fig. 5). Above these limiting temperatures EPR lines vanish. As one can see EPR lines originating from LN:Yb^{3+}, Pr^{3+} crystal have got higher intensity values than these of LN:Yb^{3+} sample (see Fig. 4). This is some surprise to some extent, because we have found EPR spectra originating from LN:Yb^{3+} show better resolution with respect to lines originating from LN:Yb^{3+} co-doped with Pr. Additionally, in case of LN crystal doped only with Yb (1 wt.%), we have got about 20% higher concentration of ytterbium ions than in case of LN:Yb, Pr (0.8 wt.%), whereas integrated intensity had got clearly higher values for the co-doped sample, essentially at low temperature (below 25 K).

This indicates that the presence of Pr co-dopant favours incorporate of ytterbium ions being dispersed in different, available sites in host crystal. From Fig. 10 one can see the linewidth of the EPR lines originating from LN:Yb is less than in case of LN:Yb, Pr. Moreover, both crystals are distinctly different in the value of *g*-factor. The intensity of the integrated EPR lines (Fig. 10, upper figure) gradually increases when temperature decrease, shows a sharp increase at about $T = 7.2 \pm 0.2$ K for LN:Yb^{3+} and $T = 8.25 \pm 0.75$ K for LN:Yb^{3+}, Pr^{3+} crystal, and next slight decrease below 7 K.

Similarly, the temperature dependence of the inverse intensity (Fig. 11) reveals a clear deviation from the Curie–Weiss law below 7 K for both crystals, as is presented more clearly in the inset of the figure. This observation is confirmed by a very weak minimum at the same temperature in the temperature dependence of the linewidth and *g*-factor for both crystals. Fig. 11 shows complex behavior of the temperature dependence of the inverse EPR line intensity for the LN:Yb^{3+} and LN:Yb^{3+}, Pr^{3+} crystals. It should be mentioned that experimental uncertainty is less than the size of the data points.

In case of LN:Yb^{3+} sample low-temperature regions can be identified between 5 and 40 K. Unexpectedly, above the 40 K, we observe other line of very low intensity which disappear near

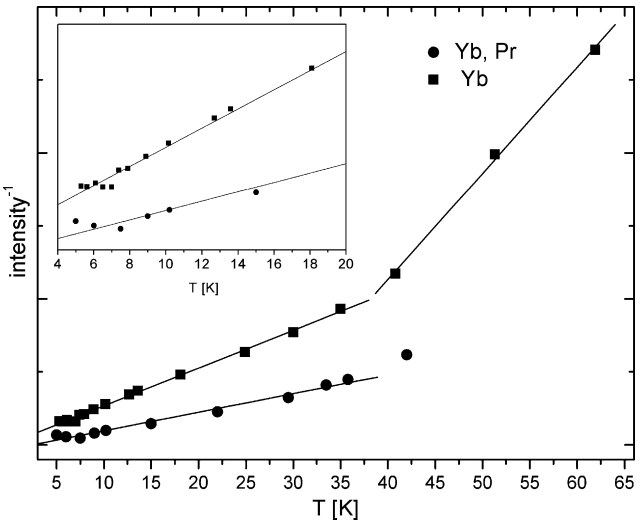

Fig. 11. Temperature dependence of the inverse EPR line intensity for the LN:Yb^{3+} (solid squares) and LN:Yb^{3+}, Pr^{3+} single crystals (solid dots). The inset shows an enlarged section of the low-temperature dependence of the inverse intensity (up to 20 K).

about 63 K. The origin of the line is not clear. At this stage we can suppose the line may originate from uncontrolled paramagnetic ions which entered the LN structure during crystal growth. We cannot determine a concentration of this unidentified impurity but undoubtedly we can say that its concentration is much less than the concentration of the Pr co-dopant in LN:Yb^{3+}, Pr^{3+} crystal.

The inverse intensity versus temperature can be described very well by Curie–Weiss law for LN:Yb^{3+} and LN:Yb^{3+}, Pr^{3+} samples, besides the very low temperature region, what can be seen in the inset. The observed behavior indicates that in the temperature region dominated by EPR lines originating from Yb^{3+} ions (5–42 K), the EPR line intensity satisfies the Curie–Weiss law for both samples. This enables us to determine the Curie temperature as being equal to $\Theta = -0.6 \pm 0.3$ K in case of LN:Yb^{3+} and $\Theta = 2.4 \pm 0.1$ K for LN:Yb^{3+}, Pr^{3+} single crystals.

Unexpected sharp increase in intensity of the EPR line in the temperature of $T = 7.2 \pm 0.2$ and 8.25 ± 0.8 K for LN:Yb^{3+} and LN:Yb^{3+}, Pr^{3+}, respectively, and the fact that EPR line intensity satisfies Curie–Weiss law for both samples, suggest the EPR lines can not origin from Yb^{3+} ions only. One of the reasons of such behavior of the EPR lines can be the presence of Yb^{3+}–Yb^{3+} ion pairs. This explanation agrees with the indications made from the optical spectroscopy measurements discussed in Section 3.1, which suggest possibility of evidence of the Yb^{3+} pairs in optical and Raman spectra.

The negative Curie temperature Θ suggests that antiferromagnetic interactions may arise in the system of Yb^{3+} ions in LN:Yb^{3+} while ferromagnetic interactions may arise in the system of Yb^{3+} ions in LN:Yb^{3+}, Pr^{3+}. Thus, the temperature behavior of the EPR intensity and its inverse may be explained by the presence of antiferromagnetically coupled Yb^{3+} ion pairs in LN:Yb^{3+} crystal and ferromagnetically coupled Yb^{3+} ion pairs in case of LN:Yb^{3+}, Pr^{3+} crystal.

4. Conclusions

We have observed much higher OH^- absorption band intensity in Pr^{3+}-doped and co-doped crystals and the increase of the intensity with increasing Pr^{3+} concentration. It suggests the substitution of Pr^{3+} ions for Nb^{5+} ions. The latter substitution leads to the octahedrons being deformed and creation of negatively charged defects of $(Pr^{3+}{}_{Nb^{5+}})^{2-}$ type that require charge compensation by positively charged $(OH^-{}_{O^{2-}})^{+}$ ones in $Yb^{3+} + Pr^{3+}$ co-doped LN crystal.

The abnormal behavior was observed for 980 nm absorption line intensity versus temperature. The intensity maximum of 980 nm line we observed at about 190 and 230 K for LN:Yb and LN:Yb, Pr, respectively. The maxima correspond to energies of about 100–300 cm^{-1}. It may be due to the existing of localized phonons in the LN crystal. This supposition was confirmed by Raman spectra investigations, where localized phonons with energy within 80–300 cm^{-1} range we have clearly observed. The dumping of 152 cm^{-1} $E(TO_1)$ mode found in the Raman spectrum of the Nd and Yb doped LN is considered to be due to the increase of Nb_{Li} concentration caused by the doping. We have assigned the 100 cm^{-1} additional Raman peak to γ-induced defect or co-doping influence (pairs), the 193 cm^{-1} peak to RE doping of LN crystal and 238 cm^{-1} peak to co-doping influence, all being localized type phonons.

We have observed several paramagnetic centers originating from both isolated Yb^{3+} and Yb^{3+} ion pairs in both LN:Yb^{3+}, Pr^{3+} and LN:Yb^{3+} crystals. The observed spectral features indicate that Yb^{3+} centers exhibit triclinic C_1 symmetry in both crystals. We have not observed paramagnetic centers with axial point group symmetry. A possible reason may be too low resolution of our EPR X-band spectrometer.

The temperature dependence of the EPR line intensity and inverse line intensity confirm the presence of coupled Yb^{3+} ion pairs besides isolated Yb ions in both crystals. The EPR line intensity fulfils the Curie–Weiss law and yields antiferromagnetic interaction constant $\Theta = (-0.6 \pm 0.3)$ K and ferromagnetic interaction constant $\Theta = (2.4 \pm 0.1)$ K for LN:Yb^{3+} and LN:Yb^{3+}, Pr^{3+} samples, respectively.

The presence of a co-dopant significantly changes properties of LN:Yb^{3+} single crystal. The Pr co-dopant forces the substitution of Yb^{3+} ions at other possible sites in the host LN crystal lattice and changes interaction between Yb ion pairs from antiferromagnetic to ferromagnetic one.

Acknowledgment

We deeply acknowledge Prof. T. Tsuboi from Faculty of Engineering, Kyoto Sangyo University, Japan, for low-temperature optical measurements.

References

[1] J.M. Cabrera, J. Olivares, M. Carrascosa, J. Ramis, R. Muller, E. Dieguez, Adv. Phys. 45 (1996) 349–392.
[2] H.E. Conzett, S.I. Stepanov, Rep. Prog. Phys. 57 (1994) 39–116.

[3] Properties of Lithium Niobate, 1989, Inspec, EMIS Datareviews Series No. 5.
[4] E. Montoya, J. Capmany, L.E. Bausa, T. Kellner, A. Diening, G. Huber, Appl. Phys. Lett. 74 (1999) 3113.
[5] J.K. Jones, J.P. de Sandro, H. Hempstead, A.C. Large, A.C. Tropper, J.S. Wilkinson, Opt. Lett. 20 (1995) 1477.
[6] S.C. Abrahams, J.M. Reddy, J.L. Bernstein, J. Phys. Chem. Solids 27 (1966) 997–1012.
[7] S.C. Abrahams, W.C. Hamilton, J.M. Reddy, J. Phys. Chem. Solids (1966) 27.
[8] A. Lorenzo, H. Jaffrezic, B. Roux, G. Boulon, J. Garcia-Sole Appl. Phys. Lett. 67 (25) (1995) 3735.
[9] L. Rebouta, P.J.M. Smulders, D.O. Boerma, F. Aguillo-Lopez, M.F. Da Silva, J.C. Soares, Phys. Rev. B 48 (1993) 3600.
[10] G. Burns, D.F. O'Kane, R.S. Title, Phys. Rev. 167 (1968) 314–319.
[11] C. Bonardi, C.J. Magon, E.A. Vidoto, M.C. Terrile, L.E. Bausa, E. Montoya, D. Bravo, A. Martin, F.J. Lopez, J. Alloys Compd. 323–324 (2001) 340–343.
[12] T. Tsuboi, S.M. Kaczmarek, G. Boulon, J. Alloys Compd. 380 (2004) 196–200.
[13] A. Ridah, P. Bourson, M.D. Fontana, G. Malovichko, J. Phys. Condens. Matter 9 (1997) 55.
[14] R. Mouras, M.D. Fontana, P. Bourson, A.V. Postnikov, J. Phys. Condens. Matter 12 (2000) 5053.
[15] R. Mouras, P. Bourson, M.D. Fontana, G. Boulon, Opt. Commun. 197 (2001) 439–444.
[16] M.N. Palatnikov, I.V. Biryukova, N.V. Sidorov, A.V. Denisov, V.T. Kalinnikov, P.G.R. Smith, V.Ya. Shur, J. Cryst. Growth 291 (2006) 390–397.
[17] K. Chen, M.S. Zhang, W.C. Chen, Q. Chen, Pergamon 43–50 (2000).
[18] H.-N. Dong, S.-Y. Wu, W.-C. Zheng, J. Phys. Chem. Solids 64 (2003) 695–699.
[19] S.H. Choh, J.H. Kim, I.W. Park, H.J. Kim, D. Choi, S.S. Kim, Appl. Magn. Reson. 24 (2003) 313–319.
[20] G. Malovichko, V. Gratchev, E. Kokanyan, O. Shirmer, Phys. Rev. B 59 (1999) 9113–9125.
[21] G. Malovichko, V. Grachev, Phys. Rev. B 62 (2000) 7779–7789.
[22] E. Montoya, O. Espeso, L.E. Bausa, J. Lumin. 87–89 (2000) 1036–1038.
[23] T. Bodziony, S.M. Kaczmarek, Opt. Mater. 29 (2007) 1440–1446.
[24] T. Bodziony, S.M. Kaczmarek, J. Hanza, Proc. SPIE 5958 (2005) 64–73.
[25] I. Pracka, M. Malinowski, A.L. Bajor, B. Surma, Z. Galazka, M. Świrkowicz, M. Możdżonek, Proc. SPIE 3178 (1997) 295.
[26] S.M. Kaczmarek, I. Pracka, Z. Mierczyk, K. Kopczyński, R. Piramidowicz, M. Malinowski, J. Kisielewski, A.O. Matkovskii, D.Yu. Sugak, Acta Phys. Pol. A 90 (1996) 411–418.
[27] G. Foulon, M. Ferriol, A. Brenier, M.T. Cohen-Adad, G. Boulon, Chem. Phys. Lett. 245 (1995) 555.
[28] A.V. Postnikov, V. Caciuc, G. Borstel, J. Phys. Chem. Sol. 61 (2000) 295–299.
[29] A. Abragam, B. Bleaney, Electron Paramagnetic Resonance of Transitions Ion, Dover, New York, 1986.
[30] V. Mehta, D. Gourier, J. Phys.: Condens. Matter 13 (2001) 4567–4578.